Mathematical Medicine and Biology (2008) **25**, 65−85
doi:10.1093/imammb/dqn004
Advance Access publication on March 21, 2008

Calcium release site ultrastructure and the dynamics of puffs and sparks

HILARY DEREMIGIO AND JEFFREY R. GROFF
Department of Applied Science, The College of William and Mary, Williamsburg, VA 23187, USA

AND

GREGORY D. SMITH†
Department of Applied Science, McGlothlin-Street Hall, Room 305, The College of William and Mary, Williamsburg, VA 23187, USA and Mathematical Biosciences Institute, Ohio State University, Columbus, OH 43210, USA

[Received on 13 August 2007; revised on 18 January 2008; accepted on 29 January 2008]

When Markov chain models of intracellular Ca^{2+}-regulated Ca^{2+} channels are coupled via a mathematical representation of a Ca^{2+} microdomain, simulated Ca^{2+} release sites may exhibit the phenomenon of 'stochastic Ca^{2+} excitability' reminiscent of Ca^{2+} puffs and sparks. Interestingly, some single-channel models that include Ca^{2+} inactivation are not particularly sensitive to channel density, so long as the requirement for inter-channel communication is satisfied, while other single-channel models that do not include Ca^{2+} inactivation open and close synchronously only when the channel density is in a prescribed range. This observation led us to hypothesize that single-channel models with Ca^{2+} inactivation would be less sensitive to the details of release site ultrastructure than models that lack a slow Ca^{2+} inactivation process. To determine if this was the case, we simulated Ca^{2+} release sites composed of instantaneously coupled Ca^{2+}-regulated Ca^{2+} channels whose random spatial locations were chosen from a uniform distribution on a disc of specified radius and compared the resulting release site dynamics to simulations with channels arranged on hexagonal lattices. Analysis of puff/spark statistics confirmed our hypothesis that puffs and sparks are less sensitive to the spatial organization of release sites when the single-channel model includes a slow inactivation process. We also investigated the validity of several different mean-field reductions that do not explicitly account for the details of release site ultrastructure. The most successful approximation maintains a distinction between each channel's substantial influence on its own stochastic gating and the collective contribution of elevated $[Ca^{2+}]$ from neighbouring channels.

Keywords: puff; spark; ultrastructure; calcium.

1. Introduction

Localized Ca^{2+} elevations known as Ca^{2+} puffs and sparks are cellular signals of great interest that arise from the cooperative activity of clusters of inositol 1,4,5-trisphosphate receptors (IP_3Rs) and ryanodine receptors (RyRs). Calcium puff and sparks are not only the building blocks of global Ca^{2+} release events in eukaryotic cells but also highly specific regulators of cellular function (Berridge, 1993, 1997, 1998; Cheng *et al.*, 1993, 1996).

†Email: greg@as.wm.edu

© The author 2008. Published by Oxford University Press on behalf of the Institute of Mathematics and its Applications. All rights reserved.

The relationship between single-channel kinetics and the dynamics of localized Ca^{2+} release is complicated by the short range of action of intracellular Ca^{2+} (Allbritton *et al.*, 1992) and the co-localization of intracellular Ca^{2+} channels at Ca^{2+} release sites on the surface of the endoplasmic reticulum (ER) or sarcoplasmic reticulum. For example, in the cortical regions (approximately 6 μm below the plasma membrane) of immature *Xenopus laevis* oocytes, IP_3Rs occur in clusters of 5–50 with inter-cluster spacing on the order of a few microns (Sun *et al.*, 1998). IP_3Rs are also clustered on the surface of the outer nuclear membrane of *Xenopus* oocytes (Mak & Foskett, 1997). Similarly, intracellular Ca^{2+} release in skeletal and cardiac myocytes is mediated by clusters of RyRs that are assembled into paracrystalline arrays of 50–250 cooperatively gating channels (Franzini-Armstrong *et al.*, 1999; Bers, 2002; Wang *et al.*, 2004; Chen-Izu *et al.*, 2006).

The spatial organization of IP_3Rs and RyRs is the basis of three distinct modes of Ca^{2+} mobilization that have been observed via confocal microfluorimetry in oocytes, cardiomyocytes and many other cell types: (1) localized Ca^{2+} elevations due to the activation of single channels that are referred to as Ca^{2+} blips or quarks depending on whether the event is mediated by IP_3Rs or RyRs (Niggli, 1999; Bootman *et al.*, 1997), (2) Ca^{2+} puffs and sparks that arise from the activation of multiple channels associated with a single Ca^{2+} release site (Cheng *et al.*, 1993; Cannell *et al.*, 1995; Yao *et al.*, 1995; Parker *et al.*, 1996) and (3) global responses such as oscillations and waves that involve multiple release sites (Dupont *et al.*, 1991; Dupont & Goldbeter, 1992, 1994; Cheng *et al.*, 1996). These three modes of Ca^{2+} release have been dubbed fundamental, elementary and global responses, respectively (Berridge, 1997).

While the expression of IP_3Rs and RyRs is organism and cell specific, there is also remarkable variability in the spatial arrangement of these intracellular channels. In contrast to the paracrystalline arrays of RyRs observed in skeletal and cardiac myocytes, RyRs are diffusely distributed throughout the ER of human embryonic kidney cells (Rossi *et al.*, 2002). In antigen-stimulated rat basophilic leukaemia cells, diffusely distributed Type 2 IP_3Rs redistribute on the ER membrane to form large isolated aggregates (Wilson *et al.*, 1998). In oligodendrocyte progenitors, IP_3Rs and RyRs co-localize within Ca^{2+} release sites (Haak *et al.*, 2001). While IP_3Rs and RyRs are both expressed in leukocytes, the intracellular distribution of the channels is variable. For instance, in monocytes, IP_3Rs are diffusely distributed throughout the cell, while RyRs are arranged in clusters (Clark & Petty, 2005). In stark contrast to the case of skeletal and cardiac myocytes, in *Xenopus* oocytes, rat basophilic leukaemia cells and many other cell types mentioned above, little is known about the details of Ca^{2+} release site ultrastructure, i.e. the precise position of intracellular Ca^{2+} channels within a given cluster.

Several groups have presented simulations (Rios & Stern, 1997; Swillens *et al.*, 1998, 1999; Stern *et al.*, 1999; Shuai & Jung, 2002, 2003; Rengifo *et al.*, 2002; Hinch, 2004; Nguyen *et al.*, 2005; Mazzag *et al.*, 2005; DeRemigio & Smith, 2005) demonstrating that Ca^{2+} puffs and sparks may arise from the cooperative activity of clusters of intracellular Ca^{2+} channels modelled as continuous-time discrete-state Markov chains; for review of simulation methods, see Colquhoun & Hawkes (1995) and Smith (2002). These calculations have established that when Ca^{2+}-regulated Ca^{2+} channel models are coupled via a time-dependent or time-independent Ca^{2+} microdomain, simulated Ca^{2+} release sites may exhibit the phenomenon of 'stochastic Ca^{2+} excitability', where the IP_3Rs or RyRs open and close in a concerted fashion. Allosteric interactions between intracellular Ca^{2+} channels may lead to synchronization (Stern *et al.*, 1999; Groff & Smith, 2007, 2008), but such direct coupling is not required (Nguyen *et al.*, 2005; DeRemigio & Smith, 2005; Swillens *et al.*, 1999). Rather, Ca^{2+} puffs and sparks can readily be observed when the coupling between single-channel models is mediated entirely via the buffered diffusion of intracellular Ca^{2+} simulated through numerical solution of a system of nonlinear reaction–diffusion equations. In the above-mentioned studies, the specific single-channel model chosen, the release site geometry and the description of the cytosolic milieu all contribute to the measured

statistics of simulated puffs and sparks such as amplitude, duration and inter-event interval. The IP_3R or RyR models used often include transitions representing fast Ca^{2+} activation and slower Ca^{2+} inactivation, two phenomena that have been repeatedly (but not uniformly) observed in single-channel recordings from planar lipid bilayer and nuclear patch experiments (Fill & Copello, 2002; Hagar *et al.*, 1998; Mak & Foskett, 1997; Moraru *et al.*, 1999; Ramos-Franco *et al.*, 1998; Bezprozvanny *et al.*, 1991).

Although the biophysical theory relating the single-channel kinetics of IP_3Rs and RyRs to the collective phenomena of Ca^{2+} puffs and sparks is not well developed, Markov chain models of coupled intracellular Ca^{2+} channels give insight into the dynamics of Ca^{2+} puffs and sparks. Several investigators have observed a requirement of significant inter-channel communication in the genesis of Ca^{2+} puffs and sparks, i.e. low-density Ca^{2+} release sites exhibit a low puff-to-blip ratio or may not exhibit stochastic excitability at all (Swillens *et al.*, 1999). The stochastic Ca^{2+} excitability exhibited by coupled Ca^{2+} channels that include both Ca^{2+} activation and Ca^{2+} inactivation can be eliminated by modifying Ca^{2+} inactivation rates. In previous work, we have found that a four-state IP_3R model with Ca^{2+} inactivation is not particularly sensitive to the density of channels when these channels are regularly arranged on a hexagonal lattice at simulated release sites, so long as the requirement for inter-channel communication is satisfied. In this same study, we found that two-state channels that did not include Ca^{2+} inactivation will open and close in a synchronous fashion only when the channel density is in a prescribed range (Nguyen *et al.*, 2005). This observation led us to hypothesize that single-channel models that include Ca^{2+} inactivation would be less sensitive to the details of release site ultrastructure than single-channel models that lack a slow Ca^{2+} inactivation process.

To determine if this was the case, we considered a two-state Markov chain model of a Ca^{2+}-activated intracellular Ca^{2+} channel (Section 2.1) and, for comparison, two different three-state single-channel models. Both three-state models include fast Ca^{2+}-dependent activation; however, one contains Ca^{2+}-dependent inactivation (Section 2.2), while the other has a Ca^{2+}-independent inactivation process (Section 2.3). When these single-channel models were instantaneously coupled via reaction–diffusion equations representing the buffered diffusion of intracellular Ca^{2+}, the resulting Ca^{2+} release site models exhibited stochastic Ca^{2+} excitability reminiscent of Ca^{2+} puff and sparks (Sections 2.4, 2.5 and 3.1). To test our hypothesis that Ca^{2+} puffs and sparks are less sensitive to the spatial organization of release sites when the single-channel model includes a slow Ca^{2+} inactivation process, we performed simulations where the channels were arranged randomly according to a uniform distribution on a disc of specified radius and compared these results to simulations with channels arranged on hexagonal lattices with functionally equivalent inter-channel distances (Sections 3.2 and 3.3). In addition to confirming our hypothesis, these simulations provided an opportunity to investigate the validity of several different mean-field approximations to Ca^{2+} release site dynamics that do not explicitly account for the details of release site ultrastructure (Section 3.4).

2. Formulation of model

2.1 *A two-state channel model with Ca^{2+} activation*

Stochastic models of single-channel gating often take the form of continuous-time discrete-state Markov processes (Colquhoun & Hawkes, 1995; Smith, 2002). For example, a state transition diagram for a two-state channel activated by Ca^{2+} is given by

$$\text{(closed)}\ \mathcal{C} \underset{k^-}{\overset{k^+ c_\infty^\eta}{\rightleftharpoons}} \mathcal{O}\ \text{(open)}, \tag{2.1}$$

where $k^+c_\infty^\eta$ and k^- are transition rates with units of reciprocal time, k^+ is an association rate constant with units of conc$^{-\eta}$ time^{-1}, η is the cooperativity of Ca^{2+} binding and c_∞ is the fixed local background $[Ca^{2+}]$.

We write the stationary (time-independent) probability of being in state i as π_i and the stationary probability distribution as the row vector $\boldsymbol{\pi} = (\pi_\mathcal{C}, \pi_\mathcal{O})$. The stationary distribution satisfies both conservation of probability $\left(\sum_i \pi_i = 1\right)$ and global balance, i.e. the probability fluxes into and out of each state are equal,

$$\sum_{i \neq j} \pi_i q_{ij} = \pi_j \sum_{i \neq j} q_{ji}. \tag{2.2}$$

These conditions can be written compactly as

$$\boldsymbol{\pi}\, Q = \mathbf{0} \quad \text{subject to } \boldsymbol{\pi}\, \boldsymbol{e} = 1, \tag{2.3}$$

where $\boldsymbol{\pi}\, \boldsymbol{e}$ is an inner product and $\boldsymbol{e}$ is a commensurate column vector of 1s. Thus, for a two-state channel activated by Ca^{2+}, $\pi_\mathcal{C} + \pi_\mathcal{O} = 1$ and

$$\pi_\mathcal{C} = \frac{k^-}{k^+c_\infty^\eta + k^-} = \frac{K^\eta}{c_\infty^\eta + K^\eta}, \quad \pi_\mathcal{O} = \frac{k^+c_\infty^\eta}{k^+c_\infty^\eta + k^-} = \frac{c_\infty^\eta}{c_\infty^\eta + K^\eta}, \tag{2.4}$$

where $K^\eta = k^-/k^+$. Figure 1(A) (dotted line) shows that the open probability ($\pi_\mathcal{O}$) of this two-state channel model increases with higher background $[Ca^{2+}]$ (c_∞) and, because there is no Ca^{2+} inactivation present in the single-channel model, $\pi_\mathcal{O} \to 1$ as $c_\infty \to \infty$.

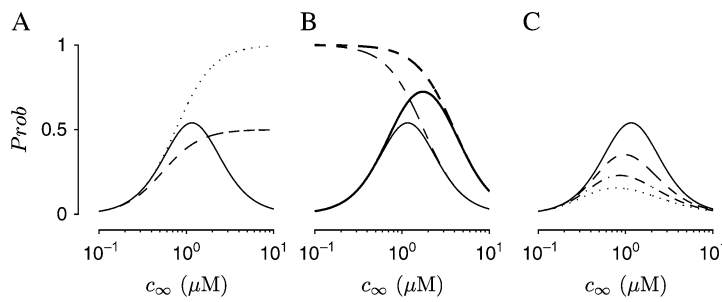

FIG. 1. (A) Steady-state open probability $\pi_\mathcal{O}$ of the two-state model (dotted line), three-state model with Ca^{2+} inactivation (solid line) and three-state model with Ca^{2+}-independent inactivation (dashed line) given by (2.4), (2.6) and (2.9), respectively, as functions of the background $[Ca^{2+}]$ (c_∞). Two-state model parameters: $\eta = 2$, $k^+ = 1.5$ μM^{-2} ms^{-1} and $k^- = 0.5$ ms^{-1}. Three-state model with Ca^{2+}-dependent inactivation parameters: $\eta = 2$, $k_a^+ = 1.5$ μM^{-2} ms^{-1}, $k_a^- = 0.5$ ms^{-1}, $k_b^+ = 0.001$ μM^{-2} ms^{-1} and $k_b^- = 0.01$ ms^{-1}. Three-state model with Ca^{2+}-independent inactivation parameters: $\eta = 2$, $k_a^+ = 1.5$ μM^{-2} ms^{-1}, $k_a^- = 0.5$ ms^{-1} and $\bar{k}_b^+ = \bar{k}_b^- = 0.01$ ms^{-1}. (B) $\pi_\mathcal{O}$ of the three-state model with Ca^{2+}-dependent inactivation for two different dissociation constants (K_b) for Ca^{2+}-mediated inactivation. Using $K_b = 3.16$ μM, the thin solid line shows $\pi_\mathcal{O}$ and the thin dashed line shows the steady-state probability that the channel is not refractory ($1 - \pi_\mathcal{R} = \pi_\mathcal{O} + \pi_\mathcal{C}$). The thick solid and dashed lines show $\pi_\mathcal{O}$ and $1 - \pi_\mathcal{R}$ for $K_b = 15.8$ μM. (C) $\pi_\mathcal{O}$ of the three-state single-channel model with Ca^{2+} inactivation for $K_b = 3.16$ μM and different domain Ca^{2+} concentrations: $c_d = 0$ (solid line), 1 (dashed line), 2 (dot-dashed line) and 3 μM (dotted line). Other parameters as in (B).

2.2 *A three-state channel model with Ca^{2+} activation and Ca^{2+} inactivation*

A state transition diagram for a three-state channel model with both fast Ca^{2+} activation ($\mathcal{C} \to \mathcal{O}$) and slower Ca^{2+}-mediated inactivation ($\mathcal{O} \to \mathcal{R}$) is

$$\mathcal{C} \underset{k_a^-}{\overset{k_a^+ c_\infty^\eta}{\rightleftharpoons}} \mathcal{O} \underset{k_b^-}{\overset{k_b^+ (c_\infty + c_\mathrm{d})^\eta}{\rightleftharpoons}} \mathcal{R}, \tag{2.5}$$

where $\mathcal{R}$ corresponds to a long-lived closed state. Assuming that Ca^{2+} microdomain formation and collapse are fast processes compared to channel gating (Nguyen *et al.*, 2005; Mazzag *et al.*, 2005), the Ca^{2+}-mediated transition rate out of the open state is given by $k_b^+(c_\infty + c_\mathrm{d})^\eta$, where c_∞ is the background $[Ca^{2+}]$ and c_d is the domain $[Ca^{2+}]$, i.e. the increase in local $[Ca^{2+}]$ above background experienced by the Ca^{2+} regulatory site when the channel is open.

When the channel is not conducting Ca^{2+}, the domain $[Ca^{2+}]$ is zero ($c_\mathrm{d} = 0$) and the steady-state probability distribution of the three-state model is

$$\pi_\mathcal{C} = \frac{K_a^\eta K_b^\eta}{D}, \quad \pi_\mathcal{O} = \frac{K_b^\eta c_\infty^\eta}{D}, \quad \pi_\mathcal{R} = \frac{c_\infty^{2\eta}}{D}, \tag{2.6}$$

where $K_i^\eta = k_i^- / k_i^+$ for $i \in \{a, b\}$ and $D = K_a^\eta K_b^\eta + K_b^\eta c_\infty^\eta + c_\infty^{2\eta}$. The solid line in Fig. 1(A) shows how the open probability of the three-state channel increases and then decreases with increasing background $[Ca^{2+}]$. This is due to the Ca^{2+} inactivation present in the single-channel model which causes $\pi_\mathcal{O} \to 0$ and $\pi_\mathcal{R} \to 1$ as $c_\infty \to \infty$. For the three-state single-channel model with both Ca^{2+} activation and Ca^{2+} inactivation, Fig. 1(B) shows the steady-state open probability given by (2.6) for two different values of the dissociation constant for Ca^{2+} inactivation (K_b). The thin solid and dashed lines show the steady-state open probability ($\pi_\mathcal{O}$) and the steady-state probability that the channel is not refractory ($1 - \pi_\mathcal{R} = \pi_\mathcal{O} + \pi_\mathcal{C}$) as a function of background $[Ca^{2+}]$ using K_b = 3.16 μM. For comparison, the thick solid and dashed lines show $\pi_\mathcal{O}$ and $1 - \pi_\mathcal{R}$ when the dissociation constant for inactivation is increased five-fold (K_b = 15.8 μM).

When Ca^{2+} is the current carrier, the domain $[Ca^{2+}]$ is positive ($c_\mathrm{d} > 0$) and the steady-state probability distribution of the three-state model is given by

$$\pi_\mathcal{C} = \frac{K_a^\eta K_b^\eta}{D}, \quad \pi_\mathcal{O} = \frac{K_b^\eta c_\infty^\eta}{D}, \quad \pi_\mathcal{R} = \frac{c_\infty^\eta (c_\infty + c_\mathrm{d})^\eta}{D}, \tag{2.7}$$

where $K_i^\eta = k_i^- / k_i^+$ for $i \in \{a, b\}$ and $D = K_a^\eta K_b^\eta + K_b^\eta c_\infty^\eta + c_\infty^\eta (c_\infty + c_\mathrm{d})^\eta$. Figure 1(C) shows how changing the value of the domain Ca^{2+} concentration (c_d) affects the steady-state open probability of the three-state model. Increasing c_d from 0 (solid line) to more elevated values (broken lines) decreases the bell-shaped steady-state open probability curve for all values of the bulk $[Ca^{2+}]$ (c_∞).

2.3 *A three-state channel model with Ca^{2+}-independent inactivation*

For comparison to the model presented in Section 2.2, some simulations will include a three-state channel model with fast Ca^{2+} activation and slower Ca^{2+}-independent inactivation given by

$$\mathcal{C} \underset{k_a^-}{\overset{k_a^+ c_\infty^\eta}{\rightleftharpoons}} \mathcal{O} \underset{\bar{k}_b^-}{\overset{\bar{k}_b^+}{\rightleftharpoons}} \mathcal{R}, \tag{2.8}$$

where $\mathcal{R}$ again corresponds to a long-lived closed state, but the $\mathcal{O} \to \mathcal{R}$ transition does not require binding of Ca^{2+}. Under the assumption of fast Ca^{2+} microdomain formation and collapse, the steady-state open probability of this model does not depend on the domain $[Ca^{2+}]$ (c_d) and is given by

$$\pi_{\mathcal{C}} = \frac{K_a^{\eta}\bar{K}_b}{D}, \quad \pi_{\mathcal{O}} = \frac{\bar{K}_b c_{\infty}^{\eta}}{D}, \quad \pi_{\mathcal{R}} = \frac{c_{\infty}^{\eta}}{D}, \tag{2.9}$$

where $K_a^{\eta} = k_a^- / k_a^+$, $\bar{K}_b = \bar{k}_b^- / \bar{k}_b^+$ and $D = K_a^{\eta}\bar{K}_b + \bar{K}_b c_{\infty}^{\eta} + c_{\infty}^{\eta}$. The dashed line in Fig. 1(A) shows how the open probability of the three-state channel increases with increasing background $[Ca^{2+}]$ to the maximum steady-state open probability of $\bar{K}_b/(1 + \bar{K}_b) = 0.5$.

2.4 *Coupled Ca^{2+}-regulated Ca^{2+} channels*

In our initial model formulation, the interaction between channels in the Ca^{2+} release site model is mediated through the buffered diffusion of intracellular Ca^{2+} (Nguyen *et al.*, 2005). Each channel contributes to the $[Ca^{2+}]$ profile throughout the Ca^{2+} release site—the so-called Ca^{2+} microdomain—and influences the local $[Ca^{2+}]$ experienced by other channels (see Fig. 2). As in the case of the single-channel models presented above, we assume that the formation and collapse of individual peaks within the Ca^{2+} microdomain occur quickly compared to channel gating. We also assume that the validity of superposing local $[Ca^{2+}]$ increases due to each of the N channels (Naraghi & Neher, 1997; Smith *et al.*, 2001). Thus, channel interactions can be summarized by an $N \times N$ 'coupling matrix' $\mathbf{C} = (c_{ij})$ that gives the increase over c_{∞} experienced by channel j when channel i is open. The diagonal elements of $\mathbf{C}$ represent the quantity denoted above as domain $[Ca^{2+}]$ (c_d), the increase in $[Ca^{2+}]$ above background that an open channel contributes to its own Ca^{2+} regulatory site (Nguyen *et al.*, 2005).

To specify the values of the coupling matrix $\mathbf{C}$, we assume that channels are localized on a planar ER membrane ($z = 0$). If we write $\mathbf{r}_i = x_i\hat{x} + y_i\hat{y}$ as the position of the pore of channel i, then assuming one high concentration Ca^{2+} buffer, the local $[Ca^{2+}]$ at position $\mathbf{r} = x\hat{x} + y\hat{y} + z\hat{z}$ given by the 'excess buffer approximation' is (Neher, 1986; Smith *et al.*, 2001).

$$c(\mathbf{r}) = c_{\infty} + \sum_i \frac{\sigma_i}{2\pi D|\mathbf{r}_i - \mathbf{r}|} e^{-|\mathbf{r}_i - \mathbf{r}|/\lambda}, \tag{2.10}$$

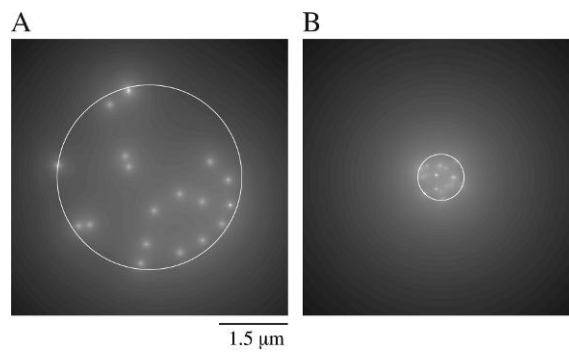

FIG. 2. (A and B) Using the excess buffer approximation (2.10), the local $[Ca^{2+}]$, $c(x, y, z = r_d)$, is shown at the level of the Ca^{2+} regulatory sites of 19 open channels with positions chosen from a uniform distribution on a disc (white circle) of radius $R = 2.0$ and 0.5 μm, respectively. Parameters used: $\sigma_{\mathcal{O}} = 0.05$ pA, $D = 250$ μM^2 s^{-1}, $\lambda = 5$ μm and $r_d = 0.05$ μm. Greyscale ranges from 50 nM (c_{∞}, black) to 100 μM (white).

where σ_i is the source amplitude of channel i, λ is the buffer length constant and D is the diffusion constant for free Ca^{2+}. If we assume identical source amplitudes,

$$\sigma_i(t) = \begin{cases} 0, & \text{channel } i \text{ closed}, \\ \sigma_{\mathcal{O}}, & \text{channel } i \text{ open}, \end{cases}$$

and write $\mathbf{a}_j$ as the position of the Ca^{2+} regulatory site for channel j, the increase in Ca^{2+} experienced by channel j when channel i is open is given by

$$c_{ij} = \frac{\sigma_{\mathcal{O}}}{2\pi D|\mathbf{r}_i - \mathbf{a}_j|} \mathrm{e}^{-|\mathbf{r}_i - \mathbf{a}_j|/\lambda}.$$

Assuming that the regulatory sites are located a small distance r_d above the channel pores, we write $\mathbf{a}_j = x_i\hat{x} + y_i\hat{y} + r_\mathrm{d}\hat{z}$ and $r_{ij} = |\mathbf{r}_i - \mathbf{a}_j|$, so $r_{ii} = |\mathbf{r}_i - \mathbf{a}_i| = r_\mathrm{d}$. Thus, the off-diagonal elements of the coupling matrix $\mathbf{C} = (c_{ij})$ are

$$c_{ij} = \frac{\sigma_{\mathcal{O}}}{2\pi D r_{ij}} \mathrm{e}^{-r_{ij}/\lambda} \quad (i \neq j) \tag{2.11}$$

and the diagonal elements of $\mathbf{C}$ are identical and given by

$$c_{ii} = c_\mathrm{d} = \frac{\sigma_{\mathcal{O}}}{2\pi D r_\mathrm{d}} \mathrm{e}^{-r_\mathrm{d}/\lambda}. \tag{2.12}$$

Note that $r_{ij} = r_{ji}$ implies that the interaction matrix is symmetric ($c_{ij} = c_{ji}$).

2.5 *Release site ultrastructure*

While the source amplitude of the channels (σ_i), the free Ca^{2+} diffusion coefficient (D) and the buffer length constant (λ) that appear in (2.10) influence the coupling matrix $\mathbf{C}$, equally important is the release site ultrastructure, i.e. the spatial location of the channels that make up a given Ca^{2+} release site. In the Ca^{2+} release site simulations that are the focus of this manuscript, channels will be regularly arranged in a hexagonal lattice as in previous work (Nguyen *et al.*, 2005) or, alternatively, channels will have positions randomly chosen from a 2D uniform distribution on a disc of radius R. Figure 2(A) shows the Ca^{2+} microdomain exhibited by an example release site with 19 randomly positioned channels ($R = 2.0$ μm). When channels are randomly arranged, it is often the case that the minimum inter-channel distance can be quite small (0.06 μm in Fig. 2A as opposed to 1 μm for a 19-channel hexagonal lattice of the same radius). Nevertheless, decreasing the release site radius for this release site with randomly positioned channels (0.5 μm in Fig. 2B) increases the average local $[Ca^{2+}]$ that channels experience when all 19 channels are open (5.28 and 12.55 μm, respectively). The observable $[Ca^{2+}]$ that could in principle be back-calculated from a confocal microfluorometric measurement corresponds to the average $[Ca^{2+}]$ in a specified volume near the release site, e.g.

$$c_\mathrm{avg}(t) = \frac{1}{4\bar{x}\bar{y}\bar{z}} \int_0^{\bar{z}} \int_{-\bar{y}}^{\bar{y}} \int_{-\bar{x}}^{\bar{x}} c(x, y, z, t)\mathrm{d}x\,\mathrm{d}y\,\mathrm{d}z, \tag{2.13}$$

where $\bar{x}$, $\bar{y}$ and $\bar{z}$ determine the extent of the spatial averaging and $c(x, y, z, t)$ depends on the state of each channel through (2.10).

3. Results

3.1 *Representative Ca^{2+} release site simulations*

Figures 3 and 4 show example simulations—performed using Gillespie's method (Gillespie, 1976)—of Ca^{2+} release sites composed of two-state (2.1) and three-state (2.5) models, respectively. Note that 19 two-state channels arranged in a hexagonal lattice lead to 2^{19} = 524,288 configurations—45,336 of which are distinguishable when accounting for rotational and reflective symmetries of the Ca^{2+} release site—but for simplicity Fig. 3 shows the number of open channels ($N_{\mathcal{O}}$) as a function of time with the understanding that the number of closed channels is given by $N_{\mathcal{C}} = N - N_{\mathcal{O}}$. Figure 3 also shows the fluctuating spatially averaged $[Ca^{2+}]$ (c_{avg}) near the release site given by (2.13) that corresponds to the observable $[Ca^{2+}]$ that could in principle be back-calculated from a confocal microfluorometric measurement. Similarly, Fig. 4 shows the time evolution of the number of open ($N_{\mathcal{O}}$) and refractory ($N_{\mathcal{R}}$) channels in a Ca^{2+} release site composed of 19 three-state channels with Ca^{2+}-dependent inactivation. Both Figs 3 and 4 exhibit stochastic Ca^{2+} excitability reminiscent of Ca^{2+} puffs/sparks, i.e. the expected number of open channels is low ($E[N_{\mathcal{O}}] = 2$), but occasionally a large number of channels open simultaneously and $N_{\mathcal{O}}$ increases to between 10 and 19.

Because there are a finite number of intracellular Ca^{2+} channels at a release site, there is always a chance that all of them will close simultaneously, a mechanism referred to as 'stochastic attrition' (Stern, 1992; Stern & Cheng, 2004; DeRemigio & Smith, 2005). Because Ca^{2+} inactivation is absent in the two-state single-channel model (2.1), the Ca^{2+} puffs/sparks shown in Fig. 3 must be terminating via stochastic attrition. In contrast, the three-state single-channel model (2.5) includes a long-lived closed (i.e. refractory) state. In simulated Ca^{2+} puffs/sparks using this model (Fig. 4), the number of

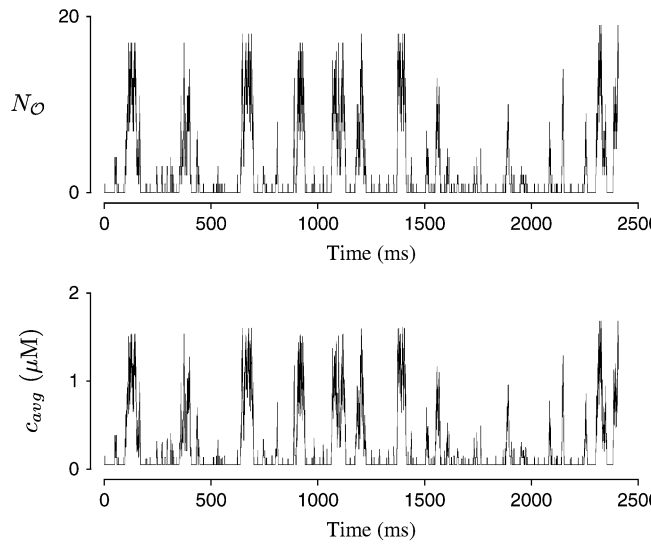

FIG. 3. Representative Ca^{2+} release site simulation using 19 two-state channels arranged on a hexagonal lattice exhibits stochastic Ca^{2+} excitability reminiscent of Ca^{2+} puffs/sparks. The time evolution of the number of open ($N_{\mathcal{O}}$) channels is plotted as well as the spatially averaged $[Ca^{2+}]$ (c_{avg}) near the release site given by (2.13). Parameters: $R = 2.15$ μm, $c_\infty = 0.1$ μM, $\sigma_{\mathcal{O}} = 0.05$ pA, $D = 250$ μM^{-2} s^{-1}, $\lambda = 5$ μm, $\eta = 2$, $k^+ = 1.5$ μM^{-2} ms^{-1}, $k^- = 0.5$ ms^{-1}, $r_{\text{d}} = 0.05$ μm, $\bar{x} = \bar{y} = R$ and $\bar{z} = R/2$. Increased source amplitude ($\sigma_{\mathcal{O}} = 0.9$ pA) and the decreased affinity for Ca^{2+} binding ($k^+ = 0.04$ μM^{-2} ms^{-1}, $k^- = 1$ ms^{-1}) result in sparks with 10-fold higher amplitude (not shown).

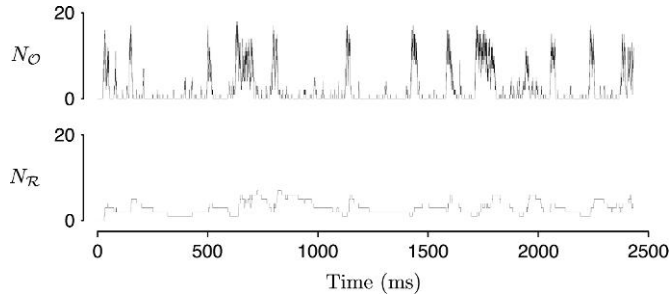

FIG. 4. Representative Ca^{2+} release site simulation using 19 three-state channels with Ca^{2+}-dependent inactivation arranged on a hexagonal lattice shows robust Ca^{2+} puffs/sparks. The time evolution of the number of open ($N_{\mathcal{O}}$) and refractory ($N_{\mathcal{R}}$) channels is shown. Parameters as in Fig. 3 with R = 1.78 μm.

refractory channels increases throughout the duration of puff/spark events, suggesting that the puff/spark termination mechanism includes Ca^{2+} inactivation as well as stochastic attrition.

To quantify the robustness of the stochastic Ca^{2+} excitability exhibited in Figs 3 and 4, we use a response measure whose value correlates well with the presence of puffs/sparks in Ca^{2+} release site simulations (Nguyen *et al.*, 2005). The puff/spark Score is the index of dispersion of the fraction of open channels given by

$$\text{Score} = \frac{1}{N}\frac{\text{Var}[N_{\mathcal{O}}]}{\text{E}[N_{\mathcal{O}}]}. \tag{3.1}$$

This Score takes values between 0 and 1, with values greater than approximately 0.3 corresponding to the presence of robust Ca^{2+} puffs/sparks. For the stochastic trajectories shown in Figs 3 and 4, the Scores are 0.40 and 0.37, respectively. Another response measure of interest is the expected fraction of open channels at the release site,

$$f_{\mathcal{O}} = \frac{1}{N}\text{E}[N_{\mathcal{O}}]. \tag{3.2}$$

3.2 *Ca^{2+} inactivation and release site dynamics—regularly arranged channels*

In Ca^{2+} release site simulations where channel positions are explicit, the radius of the release site influences puff/spark statistics such as the fraction of open channels ($f_{\mathcal{O}}$) and the Score (3.1) (Nguyen *et al.*, 2005). To determine whether Ca^{2+}-regulated channels that include Ca^{2+} inactivation are less sensitive to release site radius than Ca^{2+} channels that are activated but not inactivated by Ca^{2+}, we calculate $f_{\mathcal{O}}$ and Score as functions of R for release sites composed of two-state channels without Ca^{2+} inactivation or three-state channels with Ca^{2+}-dependent inactivation (Figs 5 and 6).

The filled circles in Fig. 5 correspond to release site simulations, where 19 two-state channels are arranged on a hexagonal lattice, while the filled and open squares show results for 19 three-state channels. Figure 5(A) shows that for release sites composed of two-state Ca^{2+}-activated channels, the fraction of open channels ($f_{\mathcal{O}}$) is an increasing function of release site density, i.e. when R is small $f_{\mathcal{O}}$ approaches 1. Conversely, the Ca^{2+}-inactivation mechanism of the three-state channel model prevents release sites from being tonically active at high density (open squares in Fig. 5A). In this case, the fraction of refractory channels ($f_{\mathcal{R}}$) increases with release site density, i.e. the three-state channels with

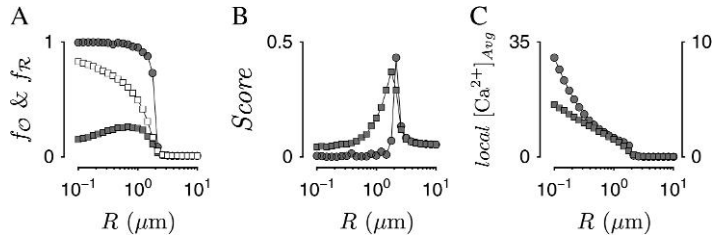

FIG. 5. Filled circles give the fraction of open channels (A), Score (B) and the increase in local $[Ca^{2+}]$ above background (C) for a Ca^{2+} release site composed of 19 two-state channels regularly arranged on a hexagonal lattice. Filled squares (alternate y-axis in (C)) give results for 19 three-state channels with Ca^{2+}-dependent inactivation, and open squares in (A) show the fraction of refractory channels. Puff statistics are plotted as a function of the release site radius R. Other parameters as in Fig. 3.

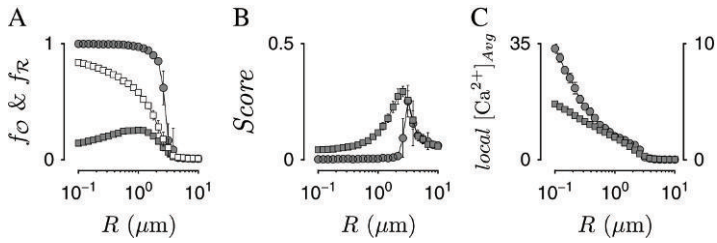

FIG. 6. Puff/spark statistics (see Fig. 5) for 19 two-state channels and three-state channels with Ca^{2+}-dependent inactivation with random positions chosen from a uniform distribution. The mean and standard deviation for 25 different release site configurations are plotted for each R. Other parameters as in Fig. 3.

both Ca^{2+} activation and Ca^{2+} inactivation tend to inactivate each other when R is small (open squares show $f_{\mathcal{R}}$ approaching 1). For both of these models, there is little Ca^{2+} excitability for release site radii larger than 2 μm ($f_{\mathcal{O}}$ approaches 0) because open channels are unable to influence the gating of their neighbours when the inter-channel distance is too large.

Figure 5(B) shows that for release sites composed of either two-state channels or three-state channels with Ca^{2+}-dependent inactivation, the puff/spark Score is a biphasic function of release site density, i.e. robust puffs/sparks are observed for intermediate values of R. However, there is a broader range of elevated Scores (above 0.3) for release sites composed of three-state as opposed to two-state channels (compare filled squares to circles). This indicates that the presence of Ca^{2+} inactivation in single-channel models can lead to Ca^{2+} release sites that are relatively insensitive to channel density.

Figure 5(C) shows the increase of local $[Ca^{2+}]$ (above background) experienced by the Ca^{2+} regulatory sites of the channels averaged over both time and channel position. At high channel density (small R), the average local $[Ca^{2+}]$ is nearly seven-fold lower for the three-state model with Ca^{2+}-dependent inactivation than the two-state model (4.5 versus 30 μM), consistent with the lower $f_{\mathcal{O}}$ and higher Score exhibited by Ca^{2+} release sites that include Ca^{2+} inactivation (Fig. 5A and B).

3.3 *Ca^{2+} inactivation and release site dynamics—randomly positioned channels*

While the puff/spark statistics of Fig. 5 were obtained from release site simulations with channels arranged in a hexagonal lattice, Fig. 6(A–C) shows $f_{\mathcal{O}}$, Score and average local $[Ca^{2+}]$ for release sites with channels randomly positioned on discs of varying radii (the mean and standard deviation for 25 different configurations are shown for each R). Interestingly, these puff/spark statistics are qualitatively

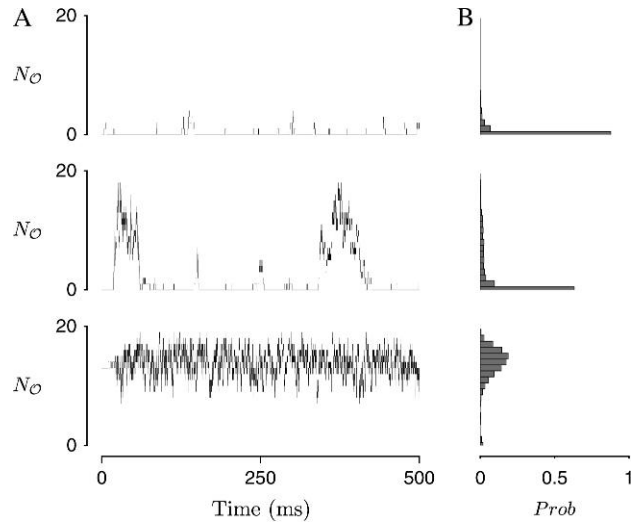

FIG. 7. (A) Representative release site simulations using 19 two-state channels randomly positioned on a disc of $R = 3.16$ μm. The time evolution of the number of open channels ($N_{\mathcal{O}}$) is shown for three trials, i.e. three different release site configurations. (B) Limiting probability distributions of the number of open channels for the three stochastic trajectories shown in (A). Other parameters as in Fig. 3.

similar to Fig. 5, suggesting that release sites that include Ca^{2+} inactivation are relatively insensitive to the details of release site ultrastructure as well as channel density.

Figure 7(A) shows representative release site simulations using 19 two-state channels in which two-state single-channel models are randomly positioned on a disc of $R = 3.16$ μm (chosen because it leads to the maximum Score of 0.34 in Fig. 6). The time evolution of the number of open channels ($N_{\mathcal{O}}$) is shown for three trials, i.e. three different release site configurations. In these release sites that do not include Ca^{2+} inactivation, the different channel positions lead to three distinct modes of release site activity including blips (top panel), robust puffs/sparks (middle) and a tonically active release site (bottom). The histograms of Fig. 7(B) are estimates of the steady-state probability distribution of the number of open channels ($\hat{\boldsymbol{\pi}}$), i.e. the nth element of $\hat{\boldsymbol{\pi}}$ is defined by

$$\hat{\pi}_n = \mathsf{P}\{N_{\mathcal{O}} = n\}, \quad 0 \leqslant n \leqslant N.$$

These histograms correspond to puff/spark Scores of 0.12, 0.36 and 0.21, respectively.

For comparison, Fig. 8(A) shows representative release site simulations using three randomly chosen spatial distributions of 19 three-state channels with Ca^{2+}-dependent inactivation (in this case the optimal R of 2.61 μm gives a Score of 0.33). In these release site simulations, robust puff/spark activity is observed in spite of the different channel positions used in each trial. In particular, note the similarity of the histograms of Fig. 8(B) with Scores in the comparatively narrow range 0.30–0.34 (cf. Fig. 7B). Interestingly, Fig. 9 shows that release sites composed of three-state channels with Ca^{2+}-independent inactivation are also relatively insensitive to the location of individual channels (here R = 2.61 μm leads to an average Score of 0.31).

Figure 10(A) shows histograms of the observed fraction of open channels ($f_{\mathcal{O}}$) and Score when 19 two-state channels are randomly positioned on a disc of optimal radius (see above). In these release site simulations that do not include a slow inactivation process, 1000 different channel configurations

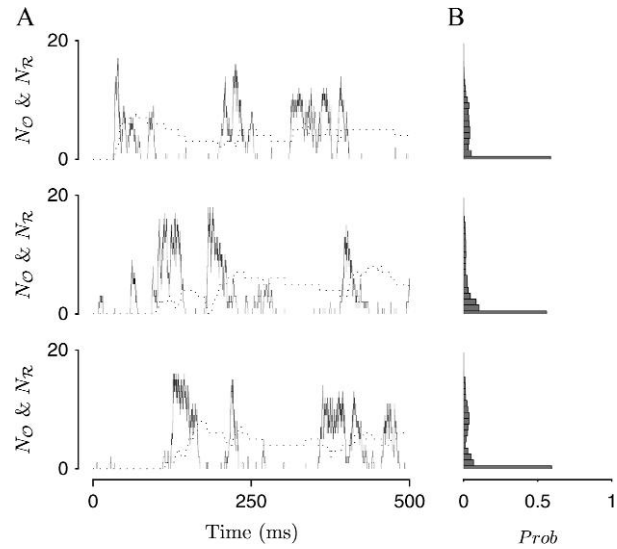

FIG. 8. (A) Representative release site simulations for 19 three-state channels with Ca^{2+}-dependent inactivation randomly positioned on a disc of $R = 2.61$ μm. The time evolution of the number of open channels (solid line) and the number of refractory channels (dotted line) is shown for three trials, i.e. three different release site configurations. (B) Limiting probability distributions of the number of open channels for the three stochastic trajectories shown in (A). Other parameters as in Fig. 3.

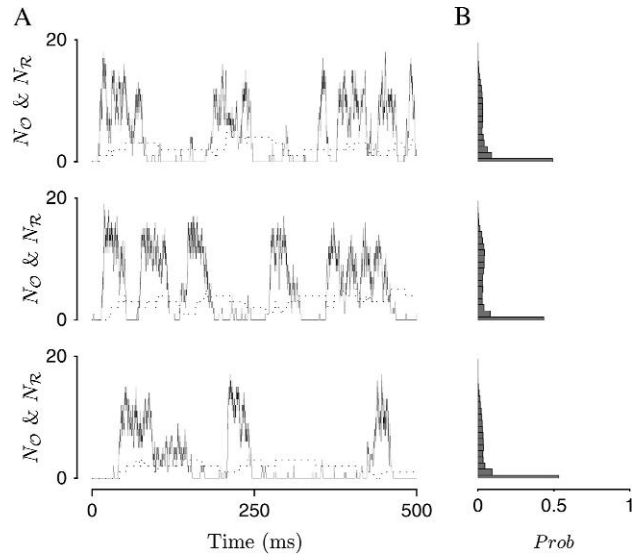

FIG. 9. (A) Representative release site simulations for 19 three-state channels with Ca^{2+}-independent inactivation randomly positioned on a disc of $R = 2.61$ μm. Other parameters as in Fig. 3. See caption of Fig. 8.

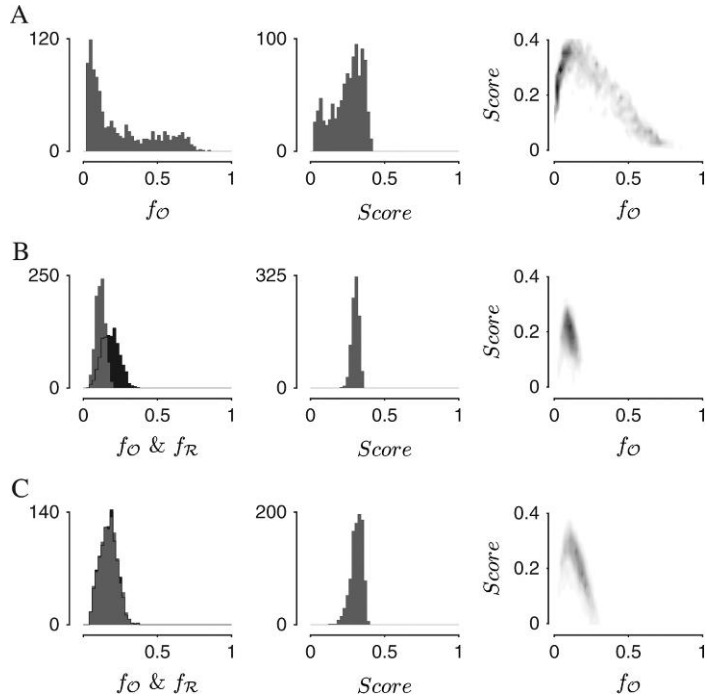

FIG. 10. (A) Histograms of observed fraction of open channels ($f_{\mathcal{O}}$, left) and Score (centre) for 1000 different release site configurations using 19 two-state channels arranged according to a uniform distribution on a disc of radius $R = 3.16$ μm. Two-dimensional plot (right) of the $f_{\mathcal{O}}$ and Score pairs obtained from the simulation results summarized in the left and centre panels. (B) Similar puff/spark statistics for 19 three-state channels with Ca^{2+} inactivation ($R = 2.61$ μm). The black histogram (left) shows the observed fraction of refractory channels ($f_{\mathcal{R}}$) for three-state channels. (C) Puff/spark statistics for 19 three-state channels with Ca^{2+}-independent inactivation ($R = 2.61$ μm). Other parameters as in Fig. 3.

result in a broad range of $f_{\mathcal{O}}$ (0.01–0.84) and Score (0.02–0.41). Conversely, Fig. 10(B) shows that release sites composed of three-state channels with Ca^{2+} inactivation display puff/spark statistics that are less variable, i.e. the observed $f_{\mathcal{O}}$ and Score are in the more restricted ranges of 0.03–0.19 and 0.20–0.35, respectively. Figure 10(C) shows that this consistency among puff/spark statistics occurs even when the slow inactivation process is Ca^{2+} independent (2.8). In this case, $f_{\mathcal{O}}$ and Score are in the restricted ranges of 0.03–0.36 and 0.12–0.37, respectively. The rightmost panels in Fig. 10(A–C) show the frequency with which blips (low $f_{\mathcal{O}}$, low Score), puffs/sparks (low $f_{\mathcal{O}}$, high Score) or a tonically active release site (high $f_{\mathcal{O}}$, low Score) occur in these 1000 channel configurations. For the optimal release site radius used here, simulations involving three-state channels with Ca^{2+}-dependent or Ca^{2+}-independent inactivation are very likely to result release site activity reminiscent of Ca^{2+} puff/sparks. Conversely, two-state channels without inactivation demonstrate a wider range of release site activity, including both blips and tonically active release, consistent with the three representative simulations presented in Fig. 7.

The spread of the open circles in Fig. 11 shows how much variability exists in release site simulations that are identical except for channel position (randomly selected from a uniform distribution on a disc of radius R). Each open circle is the ℓ^2-norm of the difference between the probability distribution of

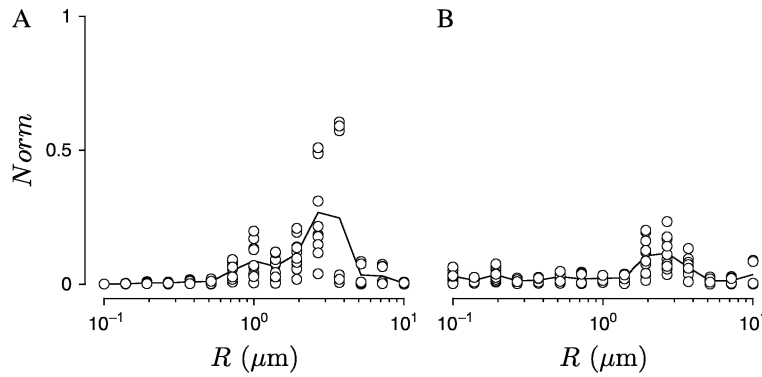

FIG. 11. (A) Open circles show the ℓ^2-norm of the difference between the probability distribution of the number of open channels for two release site simulations ($\hat{\boldsymbol{\pi}}$ and $\hat{\boldsymbol{\pi}}'$) for 19 two-state channels randomly positioned on a disc of radius R = 3.16 μm. The black line shows the average ℓ^2-norm for 10 comparisons. (B) Distributions as in (A) using 19 three-state channels with Ca^{2+}-dependent inactivation randomly positioned on a disc of radius $R = 2.61$ μm. Other parameters as in Fig. 3.

the number of open channels for two release site simulations ($\hat{\boldsymbol{\pi}}$ and $\hat{\boldsymbol{\pi}}'$), i.e.

$$\|\delta\hat{\boldsymbol{\pi}}\|_2 = \sqrt{\sum_{n=0}^{N}(\delta\pi_n)^2},$$

where $\delta\pi_n$ is the nth element of $\delta\hat{\boldsymbol{\pi}} = \hat{\boldsymbol{\pi}} - \hat{\boldsymbol{\pi}}'$. The black lines in Fig. 11 show the average ℓ^2-norm as a function of R (five configurations lead to 10 distinct comparisons for each R). For channel densities likely to lead to puffs/sparks ($2 \leqslant R \leqslant 4$ μm; see Fig. 6B), elevated average ℓ^2-norms indicate that channels without Ca^{2+} inactivation exhibit more varied activity than channels with Ca^{2+} inactivation (compare Fig. 11A and B).

3.4 *Validity of two different mean-field approximations*

Below, we investigate the validity of several different mean-field approximations to Ca^{2+} release site dynamics that do not explicitly account for the details of release site ultrastructure. In these reduced simulations, the local $[Ca^{2+}]$ experienced by each channel is assumed to depend on the number of open channels at the Ca^{2+} release site, as though the channels were indistinguishable. While prior work has shown that mean-field release site simulations result in puff/spark statistics that well approximate the dynamics of release sites with regularly arranged channels (Nguyen *et al.*, 2005), the variability observed in simulations with randomly positioned channels (Figs 7–11) led us to investigate the validity of mean-field reductions for release sites with irregular ultrastructure.

Figure 12(A and B) shows the probability distribution of the number of open channels ($N_{\mathcal{O}}$, black bars) for 19 two-state channels and three-state channels with Ca^{2+} inactivation arranged on hexagonal lattices of optimal radii ($R = 2.15$ and 1.78 μm, respectively). These simulations used a spatially explicit coupling matrix $\mathbf{C} = (c_{ij})$ (2.10) and should be considered the 'correct' result. For comparison, Fig. 12(A and B) repeats these simulations using a mean-field approximation (white bars), where the

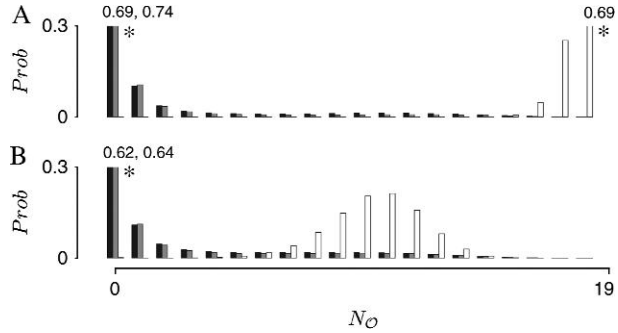

FIG. 12. (A) Black, white and grey bars show the probability distribution of the number of open two-state channels for a Ca^{2+} release site simulated using the full model (hexagonal lattice with $R = 2.15$ μm, (2.10)), Type 1 mean-field approximation (3.3) and Type 2 mean-field approximation (3.4). (B) Statistics as in (A) for three-state channels with Ca^{2+}-dependent inactivation ($R = 1.78$ μm). Other parameters as in Fig. 3.

local $[Ca^{2+}]$ experienced by each channel is

$$c = c_\infty + \bar{c} N_{\mathcal{O}}, \quad \text{where } \bar{c} = \frac{1}{N^2} \sum_{i,j} c_{ij}. \tag{3.3}$$

Note that this mean-field reduction (white bars) tends to disagree with the spatially explicit release site simulation (black bars) for both single-channel models used; in particular, they severely overestimate the fraction of open channels at the release site.

Figure 12(A and B) also shows the results of an alternative mean-field approximation (grey bars) that maintains a distinction between each channel's substantial influence on its own stochastic gating and the collective contribution of elevated $[Ca^{2+}]$ from neighbouring channels, i.e. the local $[Ca^{2+}]$ experienced by each channel is given by

$$c = \begin{cases} c_\infty + N_{\mathcal{O}} c_*, & \text{when closed,} \\ c_\infty + c_{\mathrm{d}} + (N_{\mathcal{O}} - 1) c_*, & \text{when open,} \end{cases} \tag{3.4}$$

where

$$c_* = \frac{1}{N(N-1)} \sum_{i \neq j} c_{ij} \quad \text{and} \quad c_{\mathrm{d}} = c_{ii}.$$

For both single-channel models used, this alternative mean-field approximation appears to work well (compare grey and black bars).

Let us refer to the original mean-field approximation given by (3.3) as 'Type 1' approximation, while the alternative that treats domain Ca^{2+} in a special way as 'Type 2' (3.4). To determine if Type 2 mean-field approximation is generally superior to Type 1, Fig. 13 presents simulation results for Ca^{2+} release sites with randomly positioned channels and a range of radii. The open (Type 1) and filled (Type 2) circles of Fig. 13 show the ℓ^2-norm of the difference between the probability distribution of the number of open channels for two release site simulations ($\hat{\boldsymbol{\pi}}$ and $\hat{\boldsymbol{\pi}}_{\mathrm{app}}$), where $\hat{\boldsymbol{\pi}}$ is obtained using a spatially explicit release site and $\hat{\boldsymbol{\pi}}_{\mathrm{app}}$ is one of the mean-field approximations. The black lines of Fig. 13 give the average ℓ^2-norm obtained from 10 random release site configurations.

Figure 13(A and B) shows that for both two-state channels with Ca^{2+} activation and three-state channels with both Ca^{2+} activation and Ca^{2+} inactivation, Type 2 approximation results in smaller

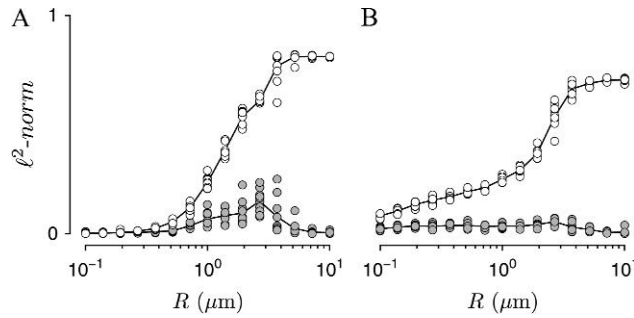

FIG. 13. (A) Open circles show ℓ^2-norm of the difference between the probability distribution of the number of open channels for two release site simulations ($\hat{\boldsymbol{\pi}}$ and $\hat{\boldsymbol{\pi}}_{\text{app}}$), where $\hat{\boldsymbol{\pi}}$ is obtained using a spatially explicit release site where 19 two-state channels randomly positioned on a disc of radius R and $\hat{\boldsymbol{\pi}}_{\text{app}}$ assumes Type 1 mean-field approximation (3.3). Filled circles show results for Type 2 mean-field approximation (3.4). Black lines show the average ℓ^2-norm for 10 release site configurations. (B) Statistics as in (A) for 19 three-state channels with Ca^{2+}-dependent inactivation. Other parameters as in Fig. 3.

ℓ^2-norms than Type 1 approximation over the entire range of release site radii considered, indicating that this approximation usually works best. Type 1 mean-field approximation becomes inaccurate at large release site radii (open circles), presumably because including the contribution of domain Ca^{2+} (c_{ii} in (3.3)) in the calculation of $\bar{c}$ leads to an overestimate of the rate of Ca^{2+}-mediated transitions out of closed states. While Type 2 approximation is generally superior to Type 1 regardless of the single-channel model used or release site ultrastructure, it performs better in the case of the three-state channels described in (2.5).

4. Discussion

In this paper, we have investigated whether single-channel models that include Ca^{2+}-dependent or Ca^{2+}-independent inactivation are less sensitive to the details of release site ultrastructure than single-channel models that lack a slow inactivation process. We limited our study to three single-channel models—a two-state model with Ca^{2+} activation but no Ca^{2+} inactivation (2.1) and two three-state models with Ca^{2+} activation and either a slow Ca^{2+}-dependent or a Ca^{2+}-independent inactivation process ((2.5) and (2.8), respectively). Consistent with previous work (Nguyen *et al.*, 2005), we have found that simulated Ca^{2+} release sites with two- or three-state channels regularly arranged on a hexagonal lattice exhibit stochastic Ca^{2+} excitability reminiscent of Ca^{2+} puffs/sparks when the release site radius is in a prescribed range (see Figs 3 and 4).

Quantitative estimates of the range of release site radii that lead to puffs/sparks will depend on the parameters chosen for the equations for the buffered diffusion of intracellular Ca^{2+}, the source amplitude of the channels and the single-channel model (see Fig. 2). One important qualitative observation in our simulations of Ca^{2+} puffs/sparks is the requirement of significant inter-channel communication for release sites to exhibit stochastic Ca^{2+} excitability (Swillens *et al.*, 1999; Nguyen *et al.*, 2005). Interestingly, the observed range of elevated Scores (3.1) for release sites composed of regularly arranged three-state channels with Ca^{2+} inactivation is broader than that observed for two-state channels with Ca^{2+}-dependent activation but no inactivation (Fig. 5B). In the case of three-state channels, the Score drops more slowly as the release site radius decreases, indicating that release sites composed of channels that include Ca^{2+} inactivation are less likely to become tonically active than release sites composed of two-state channels.

This paper establishes that the above-mentioned results generalize for release sites with random channel positions chosen from a uniform distribution on a disc of radius R (Fig. 6B), a finding that is significant because the details of Ca^{2+} release site ultrastructure are unknown for most cell types (see Section 1). In simulations where the release site radius was chosen to maximize the puff/spark Score, we found that two-state channels without Ca^{2+} inactivation exhibit more varied activity than three-state channels with either Ca^{2+}-dependent or Ca^{2+}-independent inactivation (Figs 7–9). These observations and the histograms of $f_{\mathcal{O}}$ and Score for release sites composed of irregularly arranged two- and three-state channels (Fig. 10) have confirmed our hypothesis that single-channel models with Ca^{2+} inactivation are indeed less sensitive to the details of release site ultrastructure than single-channel models that lack a slow Ca^{2+} inactivation process. Interestingly, we also observed that Ca^{2+}-dependent inactivation is not required for this insensitivity to release site ultrastructure, i.e. a slow Ca^{2+}-independent inactivation process is sufficient to allow channels to be relatively insensitive to release site ultrastructure (Fig. 9).

4.1 *Mean-field coupled Ca^{2+} channels*

The two mean-field approximations considered here neglect release site spatial organization and instead assume that the local $[Ca^{2+}]$ experienced by each channel is a function of the number of open channels (Type 1, (3.3)) or the current state of the channel and the number of open 'neighbours' (Type 2, (3.4)). Such mean-field approximations are important because they can relieve the state-space explosion that occurs when N M-state single-channel models are coupled. While a spatially explicit release site model will have M^N distinct states, the mean-field reductions that assume indistinguishable channels result in a contracted state space of size $(N + M - 1)!/(N!(M - 1)!)$. Although mean-field reductions are often used in release site simulations either for convenience or out of necessity—e.g. when directly calculating the stationary distribution from the generator matrix of the release site—it is not generally recognized that both Type 1 and Type 2 approximations are possibilities (Sobie *et al.*, 2002; DeRemigio & Smith, 2005).

In prior work, we showed that mean-field results obtained using Type 2 reduction agree with puff/spark statistics from a spatially explicit release site simulation when channels are regularly arranged in a hexagonal lattice (Nguyen *et al.*, 2005). Consistent with this prior work, we found that Type 2 mean-field approximation is a valid reduction technique for release sites with regularly arranged two-state channels with Ca^{2+} activation and three-state channels with Ca^{2+}-dependent activation and inactivation (Fig. 12). Importantly, we also were able to validate Type 2 approximation for release sites with random channel positions (Fig. 13). For the three-state model with Ca^{2+}-dependent inactivation, we found Type 1 mean-field approximation to be inferior to Type 2, presumably because it is important to distinguish between a channel's influence on its own gating (c_{d}) and the contribution from open neighbours ($c_*(N_{\mathcal{O}} - 1)$) in this case. However, for the three-state model with Ca^{2+}-independent inactivation (2.8) and no Ca^{2+}-mediated $\mathcal{O} \to \mathcal{R}$ transition, Type 1 and Type 2 mean-field approximations performed equally well (not shown).

4.2 *Timescale of Ca^{2+} inactivation*

Our simulations indicate that the presence of slow Ca^{2+} inactivation in a single-channel model causes release site dynamics to be less sensitive to channel position. In these simulations, the dissociation constant for Ca^{2+} inactivation was approximately five-fold larger than that of Ca^{2+} activation ($K_b/K_a = 5.5$, (2.5)). When the rate of the $\mathcal{R} \to \mathcal{O}$ transition (k_b^-) is decreased so that $K_b/K_a = 2.75$ (not

shown), puff/spark statistics are largely unchanged, i.e. there is a broad range of R values leading to Ca^{2+} puffs/sparks as in Fig. 6, in spite of the fact that the dwell time associated with the refractory state is much longer. Conversely, doubling k_b^- so that $K_b/K_a = 11$ leads to shorter refractory state dwell times and puff/spark statistics reminiscent of the two-state results shown in Fig. 6. Similarly, when the three-state model includes Ca^{2+}-independent inactivation (2.8), we find that puff/spark statistics are influenced by the timescale of the inactivation process. For example, when $\bar{k}_b^- = 0.01$ ms^{-1}, we observe both broad ($\bar{k}_b^+ = 0.01$ ms^{-1}) and narrow ($\bar{k}_b^+ = 0.001$ ms^{-1}) ranges of R leading to Ca^{2+} puffs/sparks depending on parameters (recall Fig. 6B). Thus, the timescale of the inactivation process and its dissociation constant determine the sensitivity of puffs/sparks to the density of channels, for both Ca^{2+}-dependent and Ca^{2+}-independent inactivation.

4.3 *Limitations to the study*

Single-channel models of IP_3Rs and RyRs can be significantly more complicated than the two- and three-state models that are the focus of this manuscript. For example, a recent IP_3R model includes 14 states, six of which are open (Fraiman & Dawson, 2004), and the well-known De Young–Keizer IP_3R model includes four eight-state subunits for a total of 330 distinguishable states (De Young & Keizer, 1992). In simulations of release sites composed of 19 four-state Type 1-like IP_3Rs (Nguyen *et al.*, 2005), puff/spark statistics are qualitatively similar to those presented in Figs 5 and 6. This suggests that it is the presence of inactivation in a single-channel model—and not any peculiarity of the three-state single-channel models used throughout this manuscript—that influences the sensitivity of release site dynamics to channel position.

This study has focused on release site simulations where channels are arranged on a regular hexagonal lattice or, alternatively, channel positions are randomly chosen from a uniform distribution. However, when channels are arranged in a different regular pattern (e.g. a square lattice), we observe results that are consistent with Fig. 5 (not shown). Similarly, when channel positions are randomly chosen from a bivariate Gaussian distribution, we observe results qualitatively similar to Fig. 6 (not shown). Thus, the conclusion that single-channel models that include Ca^{2+}-dependent or Ca^{2+}-independent inactivation are relatively insensitive to the details of release site ultrastructure is not limited to the specific release site geometries used in this manuscript.

It is also important to recognize that the assumptions of instantaneous coupling via the excess buffer approximation (2.10) are limitations to the present study. In previous work, we have shown that when Ca^{2+}-regulated channel models such as (2.1), (2.5) and (2.8) are coupled via a time-dependent Ca^{2+} domain, the time constant for domain formation and collapse can have a strong effect on both the generation and the termination of Ca^{2+} puffs/sparks (Mazzag *et al.*, 2005; Huertas & Smith, 2007). Thus, it remains an open question whether the results presented in this paper will generalize to situations where the separation of timescales between channel kinetics and Ca^{2+} domain formation and collapse are not well separated. It is also possible that different results would be obtained for instantaneously coupled channels coupled using the rapid buffer approximation or the full equations for buffered diffusion of intracellular Ca^{2+} (Smith *et al.*, 2001).

Acknowledgements

Some of these results have previously appeared in abstract form (DeRemigio & Smith, 2007). The authors acknowledge preliminary calculations performed by Nguyen (2005). Smith gratefully acknowledges a research leave during academic year 2007–2008 supported by the College of William and Mary and a long-term visitor position at the Mathematical Biosciences Institute at Ohio State University.

Funding

National Science Foundation (0133132 and 0443843).

REFERENCES

ALLBRITTON, N., MEYER, T. & STRYER, L. (1992) Range of messenger action of Ca^{2+} ion and inositol 1,4,5-trisphosphate. *Science*, **258**, 1812–1815.

BERRIDGE, M. (1993) Inositol trisphosphate and Ca^{2+} signaling. *Nature*, **361**, 315–325.

BERRIDGE, M. (1997) Elementary and global aspects of Ca^{2+} signalling. *J. Physiol. (Lond.)*, **499**, 291–306.

BERRIDGE, M. (1998) Neuronal Ca^{2+} signaling. *Neuron*, **21**, 13–26.

BERS, D. (2002) Cardiac excitation-contraction coupling. *Nature*, **415**, 198–205.

BEZPROZVANNY, I., WATRAS, J. & EHRLICH, B. (1991) Bell-shaped Ca^{2+}-response curves of Ins(1,4,5)P3- and Ca^{2+}-gated channels from endoplasmic reticulum of cerebellum. *Nature*, **351**, 751–754.

BOOTMAN, M., BERRIDGE, M. & LIPP, P. (1997) Cooking with Ca^{2+}: the recipes for composing global signals from elementary events. *Cell*, **91**, 367–373.

CANNELL, M., CHENG, H. & LEDERER, W. (1995) The control of calcium release in heart muscle. *Science*, **268**, 1045–1049.

CHENG, H., LEDERER, M., LEDERER, W. & CANNELL, M. (1996) Ca^{2+} sparks and $[Ca^{2+}]_i$ waves in cardiac myocytes. *Am. J. Physiol.*, **270**, C148–C159.

CHENG, H., LEDERER, W. & CANNELL, M. (1993) Ca^{2+} sparks: elementary events underlying excitation-contraction coupling in heart muscle. *Science*, **262**, 740–744.

CHEN-IZU, Y., MCCULLE, S., WARD, C., SOELLER, C., ALLEN, B., RABANG, C., CANNELL, M., BALKE, C. & IZU, L. (2006) Three-dimensional distribution of ryanodine receptor clusters in cardiac myocytes. *Biophys. J.*, **91**, 1–13.

CLARK, A. J. & PETTY, H. R. (2005) Differential intracellular distributions of inositol trisphosphate and ryanodine receptors within and among hematopoietic cells. *J. Histochem. Cytochem.*, **53**, 913–916.

COLQUHOUN, D. & HAWKES, A. (1995) A Q-matrix cookbook: how to write only one program to calculate the single-channel and macroscopic predictions for any kinetic mechanism. *Single-Channel Recording* (B. Sakmann & E. Neher eds). New York: Plenum Press, pp. 589–633.

DEREMIGIO, H. & SMITH, G. (2005) The dynamics of stochastic attrition viewed as an absorption time on a terminating Markov chain. *Cell Calcium*, **38**, 73–86.

DEREMIGIO, H. & SMITH, G. (2007) The spatial organization of Ca^{2+} release sites and the dynamics of puffs and sparks. *Biophysical Society Annual Meeting Abstracts, 1211-Pos.* Baltimore, MD: Biophysical Journal.

DE YOUNG, G. & KEIZER, J. (1992) A single-pool inositol 1,4,5-trisphosphate-receptor-based model for agonist-stimulated oscillations in Ca^{2+} concentration. *Proc. Natl. Acad. Sci. USA*, **89**, 9895–9899.

DUPONT, G., BERRIDGE, M. & GOLDBETER, A. (1991) Signal-induced Ca^{2+} oscillations: properties of a model based on Ca^{2+}-induced Ca^{2+} release. *Cell Calcium*, **12**, 73–85.

DUPONT, G. & GOLDBETER, A. (1992) Oscillations and waves of cytosolic Ca^{2+}: insights from theoretical models. *Bioessays*, **14**, 485–493.

DUPONT, G. & GOLDBETER, A. (1994) Properties of intracellular Ca^{2+} waves generated by a model based on Ca^{2+}-induced Ca^{2+} release. *Biophys. J.*, **67**, 2191–2204.

FILL, M. & COPELLO, J. (2002) Ryanodine receptor calcium release channels. *Physiol. Rev.*, **82**, 893–922.

FRAIMAN, D. & DAWSON, S. (2004) A model of IP_3 receptor with a luminal Ca^{2+} binding site: stochastic simulations and analysis. *Cell Calcium*, **35**, 403–413.

FRANZINI-ARMSTRONG, C., PROTASI, F. & RAMESH, V. (1999) Shape, size, and distribution of Ca^{2+} release units and couplons in skeletal and cardiac muscles. *Biophys. J.*, **77**, 1528–1539.

GILLESPIE, D. (1976) A general method for numerically simulating the stochastic time evolution of coupled chemical reactions. *J. Comput. Phys.*, **22**, 403–434.

GROFF, J. & SMITH, G. (2007) A computational investigation of the effects of allosteric coupling between ryanodine receptors on the dynamics of Ca^{2+} sparks. *Biophysical Society Annual Meeting Abstracts, 1219-Pos*. Baltimore, MD: Biophysical Journal.

GROFF, J. & SMITH, G. (2008) Ryanodine receptor allosteric coupling and the dynamics of calcium sparks. *Biophys. J.* (in press).

HAAK, L. L., SONG, L. S., MOLINSKI, T. F., PESSAH, I. N., CHENG, H. & RUSSELL, J. T. (2001) Sparks and puffs in oligodendrocyte progenitors: cross talk between ryanodine receptors and inositol trisphosphate receptors. *J. Neurosci.*, **21**, 3860–3870.

HAGAR, R., BURGSTAHLER, A., NATHANSON, M. & EHRLICH, B. (1998) Type III IP_3 receptor channel stays open in the presence of increased Ca^{2+}. *Nature*, **396**, 81–84.

HINCH, R. (2004) A mathematical analysis of the generation and termination of calcium sparks. *Biophys. J.*, **86**, 1293–1307.

HUERTAS, M. & SMITH, G. (2007) The dynamics of luminal depletion and the stochastic gating of Ca^{2+}-activated Ca^{2+} channels and release sites. *J. Theor. Biol.*, **246**, 332–354.

MAK, D. & FOSKETT, J. (1997) Single-channel kinetics, inactivation, and spatial distribution of inositol trisphosphate (IP_3) receptors in Xenopus oocyte nucleus. *J. Gen. Physiol.*, **109**, 571–587.

MAZZAG, B., TIGNANELLI, C. & SMITH, G. (2005) The effect of residual Ca^{2+} on the stochastic gating of Ca^{2+}-regulated Ca^{2+} channels. *J. Theor. Biol*. **235**, 121–150.

MORARU, I., KAFTAN, E., EHRLICH, B. & WATRAS, J. (1999) Regulation of type 1 inositol 1,4,5-trisphosphate-gated Ca^{2+} channels by IP_3 and Ca^{2+}: simulation of single channel kinetics based on ligand binding and electrophysiological analysis. *J. Gen. Physiol.*, **113**, 837–849.

NARAGHI, M. & NEHER, E. (1997) Linearized buffered Ca^{2+} diffusion in microdomains and its implications for calculation of $[Ca^{2+}]$ at the mouth of a Ca^{2+} channel. *J. Neurosci.*, **17**, 6961.

NEHER, E. (1986) Concentration profiles of intracellular Ca^{2+} in the presence of diffusible chelator. *Exp. Brain Res.*, **14**, 80–96.

NGUYEN, V. (2005) *The Dynamics of Ca^{2+} Puffs: A Study of Instantaneously Coupled Intracellular Ca^{2+} Channels*. Williamsburg, VA: The College of William and Mary.

NGUYEN, V., MATHIAS, R. & SMITH, G. (2005) A stochastic automata network descriptor for Markov chain models of instantaneously-coupled intracellular Ca^{2+} channels. *Bull. Math. Biol.*, **67**, 393–432.

NIGGLI, E. (1999) Localized intracellular Ca^{2+} signaling in muscle: Ca^{2+} sparks and Ca^{2+} quarks. *Annu. Rev. Physiol.*, **61**, 311–335.

PARKER, I., CHOI, J. & YAO, Y. (1996) Elementary events of IP_3-induced Ca^{2+} liberation in Xenopus oocytes: hot spots, puffs and blips. *Cell Calcium*, **20**, 105–121.

RAMOS-FRANCO, J., FILL, M. & MIGNERY, G. (1998) Isoform-specific function of single inositol 1,4,5-trisphosphate receptor channels. *Biophys. J.*, **75**, 834–839.

RENGIFO, J., ROSALES, R., GONZALEZ, A., CHENG, H., STERN, M. & RIOS, E. (2002) Intracellular Ca^{2+} release as irreversible Markov process. *Biophys. J.*, **83**, 2511–2521.

RIOS, E. & STERN, M. (1997) Ca^{2+} in close quarters: microdomain feedback in excitation-contraction coupling and other cell biological phenomena. *Annu. Rev. Biophys. Biomol. Struct.*, **26**, 47–82.

ROSSI, D., SIMEONI, I., MICHELI, M., BOOTMAN, M., LIPP, P., ALLEN, P. & SORRENTINO, V. (2002) RyR1 and RyR3 isoforms provide distinct intracellular Ca^{2+} signals in HEK 293 cells. *J. Cell Sci.*, **115**, 2497–2504.

SHUAI, J. & JUNG, P. (2002) Stochastic properties of Ca^{2+} release of inositol 1,4,5-trisphosphate receptor clusters. *Biophys. J.*, **83**, 87–97.

SHUAI, J. & JUNG, P. (2003) Optimal ion channel clustering for intracellular calcium signaling. *Proc. Natl. Acad. Sci. USA*, **100**, 506–510.

SMITH, G. (2002) Modeling the stochastic gating of ion channels. *Computational Cell Biology* (C. Fall, E. Marland, J. Wagner & J. Tyson eds). New York: Springer, pp. 291–325.

SMITH, G., DAI, L., MUIRA, R. & SHERMAN, A. (2001) Asymptotic analysis of equations for the buffered diffusion of intracellular Ca^{2+}. *SIAM J. Appl. Math.*, **61**, 1816–1838.

SOBIE, E., DILLY, K., DOS SANTOS CRUZ, J., LEDERER, W. & JAFRI, M. (2002) Termination of cardiac Ca^{2+} sparks: an investigative mathematical model of calcium-induced calcium release. *Biophys. J.*, **83**, 59–78.

STERN, M. (1992) Theory of excitation-contraction coupling in cardiac muscle. *Biophys. J.*, **63**, 497–517.

STERN, M. & CHENG, H. (2004) Putting out the fire: what terminates calcium-induced calcium release in cardiac muscle? *Cell Calcium*, **35**, 591–601.

STERN, M., SONG, L., CHENG, H., SHAM, J., YANG, H., BOHELER, K. & RIOS, E. (1999) Local control models of cardiac excitation-contraction coupling. A possible role for allosteric interactions between ryanodine receptors. *J. Gen. Physiol.*, **113**, 469–489.

SUN, X., CALLAMARAS, N., MARCHANT, J. & PARKER, I. (1998) A continuum of IP_3-mediated elementary Ca^{2+} signalling events in Xenopus oocytes. *J. Physiol.*, **509**, 67–80.

SWILLENS, S., CHAMPEIL, P., COMBETTES, L. & DUPONT, G. (1998) Stochastic simulation of a single inositol 1,4,5-trisphosphate-sensitive Ca^{2+} channel reveals repetitive openings during 'blip-like' Ca^{2+} transients. *Cell Calcium*, **23**, 291–302.

SWILLENS, S., DUPONT, G., COMBETTES, L. & CHAMPEIL, P. (1999) From Ca^{2+} blips to Ca^{2+} puffs: theoretical analysis of the requirements for interchannel communication. *Proc. Natl. Acad. Sci. USA*, **96**, 13750–13755.

WANG, S., STERN, M., RIOS, E. & CHENG, H. (2004) The quantal nature of Ca^{2+} sparks and in situ operation of the ryanodine receptor array in cardiac cells. *Proc. Natl. Acad. Sci. USA*, **101**, 3979–3984.

WILSON, B., PFEIFFER, J., SMITH, A., OLIVER, J., OBERDORF, J. & WOJCIKIEWICZ, R. (1998) Ca^{2+}-dependent clustering of inositol 1,4,5-trisphosphate receptors. *Mol. Biol. Cell*, **9**, 1465–1478.

YAO, Y., CHOI, J. & PARKER, I. (1995) Quantal puffs of intracellular Ca^{2+} evoked by inositol trisphosphate in Xenopus oocytes. *J. Physiol.*, **482**, 533–553.